▌ **Noncovalent Interactions**

Shell-by-Shell Functionalization of Inorganic Nanoparticles

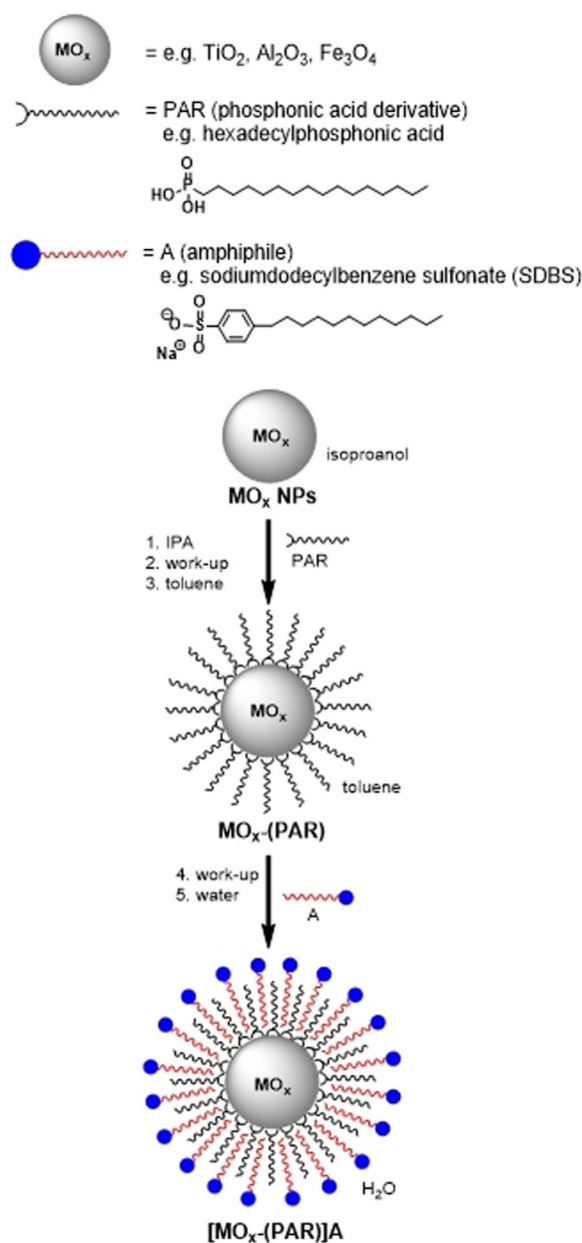Lisa M. S. Stiegler, Tobias Luchs, and Andreas Hirsch*[a]

Abstract: The current state of the hierarchical chemical functionalization of inorganic nanoparticles (NPs) by shell-by-shell (SbS)-assembly of organic layers around the NP cores is summarized. This supramolecular functionalization concept is based on two steps: 1) the covalent grafting of a first ligand–shell consisting of, for example, long chain phosphonic acids and 2) the noncovalent interdigitation of amphiphiles forming the second ligand shell. The latter process is guaranteed predominantly by solvophobic interactions. These highly order organic–inorganic hybrid architectures are currently an emerging field at the interface of synthetic chemistry, nanotechnology, and materials science. The doubly functionalized NPs display tunable materials properties, such a controlled dispersibility and stability in various solvents, highly efficient trapping of guest molecules in between the ligand shells (water cleaning) as well as compartmentalization and modification of electronic interactions between photoactive components integrated in such complex nano-architectures. Such SbS-functionalized NPs have a high potential as water-cleaning materials and also some first prototype applications as biomedicinal therapeutics have been presented.

Introduction and General Remarks

Supramolecular shell-by-shell (SbS)-functionalization of inorganic nanoparticles (NPs) has recently been established as an attractive method for the design of unprecedented dispersible hybrid architectures with tunable properties and high potential for practical applications.[1] The construction principle of such SbS-structures relies on the covalent attachment of organic ligands such as long phosphonic acid to NPs like spherical metal oxide cores, followed by the interdigitation of amphiphiles driven by solvophobic interactions (Figure 1).

First orienting approaches towards *SbS*-functionalization of NPs were already done in 1980 by Kounosu and co-workers. They used sodium dodecylbenzene sulfonate (SDBS) as a secondary adsorption layer to generate water-based magnetic fluids.[2] In 1991, Lambrick carried out studies on the double surfactant layer stabilization of water-based magnetic fluids.[3] They used C_{10}–C_{18} carboxylic acids as first and ammonium—as well as monomethyl ammonium salts of the same acids—as second layer. In 1999, Hatton developed also interdigitated bilayers to stabilize magnetic fluids, for instance by addition of *n*-alkanoic acids or cetyltrimethylammonium bromide.[4] Later in 2001 and 2003, Sastry and Yang reported the use of amphiphilic cyclodextrins as a second ligand layer to generate water dispersibility of hydrophobically coated NPs.[5] The hydrophobic cavity of the cyclodextrin is penetrated by the hydrophobic tails of the first layer and its hydrophilic surface is pointing towards the water phase. Such systems were also used as drug delivery systems for biological/medicinal/pharmaceutical applications, whereas the cavity was applied to infiltrate drugs.[6] This technique of surface-bound interdigitated bilayers using

[a] L. M. S. Stiegler, T. Luchs, Prof. Dr. A. Hirsch
    Department of Chemistry & Pharmacy
    Friedrich-Alexander-Universität Erlangen-Nürnberg
    Nikolaus-Fiebiger-Straße 10, 91058 Erlangen (Germany)
    E-mail: andreas.hirsch@fau.de

    The ORCID identification number(s) for the author(s) of this article can be found under: https://doi.org/10.1002/chem.202000195.

Figure 1. General concept of the SbS-functionalization of metal oxide NPs with a phosphonic acid as a first ligand shell and an amphiphile as a second ligand shell.

hydrophobic interactions has also been used to transfer hydrophobic gold NPs to aqueous media, for example by Sastry, Kubo and more recently by Kang and co-workers.[7] Moreover, a couple of investigations on the generation of water-dispersible quantum dots, nanocrystals or NPs for mostly biomedical applications have been reported, where additional amphiphiles or amphiphilic polymers as second shell building blocks were used.[8] Related to this, Pellegrino in 2004 described a general route towards water soluble nanocrystals via the implementation of an outer amphiphilic polymer shell.[9] In 2010, Sperling and Parak published a review on the surface modification, functionalization, and bi-conjugation of colloidal inorganic NPs.[10] They described general strategies for phase transfer of NPs from nonpolar to aqueous media, by ligand exchange reactions, but also by addition of an additional layer of amphiphilic ligand molecules or amphiphilic polymers consisting of a hydrophobic side chain and hydrophilic backbone.[10]

Our group has further exploited this construction principle and has also coined the term "shell-by-shell (SbS)-assembly".[1a–c, 11] We have recently investigated suitable building blocks for the SbS-functionalization of metal oxide NPs containing phosphonic acids as first-shell building blocks and amphiphilic molecules as second-shell building blocks for the construction of water-dispersible NP hybrid systems.[1a] That concept was further extended to three-phasic systems.[1b] Additionally, we created SbS-functionalized NPs with a tunable fluorescence towards controlling the surface morphology of a pyrene-unit on the NP surface.[1d] Furthermore, we created confined space coronas within SbS-structured NP hybrids, in which an electronic communication between organic units with different electron demand was facilitated.[11] SbS-systems could also be used as water-cleaning materials[1c] and as X-ray sensitizing agents in radiotherapy.[1e] Our Review describes first the general functionalization principle and then sets the focus on our recently published work with interesting implications and applications of such highly hierarchical ordered nano-systems.

The most frequently investigated metal oxide NP cores that have be employed in these SbS-architectures consist of TiO_2, Fe_3O_4, and Al_2O_3. The use of TiO_2 NPs allows for the introduction of semiconducting properties, which opens the door for electronic devices, such as solar cells and sensors.[12] The use of Fe_3O_4 NPs introduces magnetic properties. The size of the Fe_3O_4 NPs decides whether the NPs are ferrimagnetic or superparamagnetic.[13] By applying a magnetic field, the SbS-NPs can easily be removed from a dispersion medium by an external magnet. This has been demonstrated, for example, with the development of practical catalytic-, or water-cleaning materials.[1c, 14] Also, redox inactive Al_2O_3 NPs have been intensively investigated, for example, as core for SbS-architectures with interesting optical and electronic properties.[1d, 11] Also other types of metal oxide NPs can be used for the SbS-functionalization with phosphonic acids as anchoring groups. The SbS-functionalization concept can also be extended to other NP materials, as long as a covalent bond between the NP core and the first shell is formed to guarantee the formation of highly stable materials. Our group has demonstrated this by using silver and gold NPs together with thiols as first-shell

building blocks and the already mentioned amphiphiles as second shell building blocks.

We have presented the concept of supramolecular polarity umpolung and functionalization of SbS-coated NPs with functional amphiphiles involving systematic investigations of the colloidal behavior of such hybrid architectures in water.[1a] We have also demonstrated, that the SbS-functionalization principle of metal oxide NPs allows for the introduction of switchable dispersibility of NPs between fluorocarbon, hydrocarbon, and aqueous media by using either fluorophilic, lipophilic, or polar surfaces. This allows also for tuning of surface energies of the functionalized NPs.[1b, 15] An interesting field of application was established with ferromagnetic SbS-architectures that were used to encapsulate small nonpolar molecules from contaminated water.[1c] The hydrophobic pocket between the first and second ligand shell of the NPs was used to accommodate hydrophobic molecules. By help of an external magnet, phase separation and release of the nonpolar molecule in organic sol-

Lisa Stiegler studied Chemistry at the Friedrich-Alexander University Erlangen–Nürnberg. During her bachelor thesis she worked on fullerides and hydro-fullerides in a laboratory of the Joint Institute of Advanced Materials and Processes (ZMP) in Fürth. She performed her master thesis in a laboratory of the Engineering of Advanced Materials (EAM) Cluster while working on novel high-performance nanomaterials. Since 2016, she is working in the Chemikum in Erlangen, her research field is focused on the field of self-assembly functionalization of nanoparticles through solvophobic interactions.

Tobias Luchs studied Chemistry at the Friedrich-Alexander University Erlangen–Nürnberg. During his bachelor thesis he worked in the field of organometallic chemistry. For his master thesis he worked in a laboratory of the Engineering of Advanced Materials (EAM) Cluster. In 2016, he started as a Ph.D. candidate in the working group of Prof. Andreas Hirsch, combining inorganic nanoparticles and supramolecular chemistry for applications in energy and environmental science.

Andreas Hirsch received his doctoral degree from the University of Tübingen in 1990. He was subsequently a postdoctoral fellow at UC-Santa Barbara, USA, before he returned to Germany. In 1994, he finished his Habilitation in Organic Chemistry at the University of Tübingen. He then moved to the University of Karlsruhe to become a Professor of Organic Chemistry. Since 1995, he has been chaired Full Professor or Organic Chemistry at the University of Erlangen–Nürnberg.

vents was provided. We have also investigated electronic communication between redox-active building blocks within inter-shell interfaces and developed hybrid architectures allowing for switching on and off the emission of light.[1d] Along the same line we have reported on SbS-functionalized NPs with electronic communication between the first and second-layer interface.[11] Using a Lego-type construction principle, electron-donors were combined with electron-acceptors, which resulted in electronic communications between the molecules with different electron demand. Also, the optical properties of the NPs of the integrated chromophores were modified. Because of the excellent water dispersibility and stability of these SbS-architectures we already started to tackle some bio-medicinal applications. For this purpose hydrophobic Au–Fe_3O_4 nanohetero-dimers (NHDs) that were capped with oleic acid were encapsulated in a self-assembled bilayer shell formation with 1-octadecylpyridinium or 4-dodecylbenzenesulfonate to provide positive or negative surface charging.[1e] The surface charge as well as the surface architecture of the NHDs determine the cellular uptake, cellular localization, and the toxicity of human tumor (MCF-F7) and healthy epithelial (MCF-10A) cells. It turned out, that anionic Au–Fe_3O_4 NHDs have promising potential as X-ray sensitizing agents in radiotherapy.

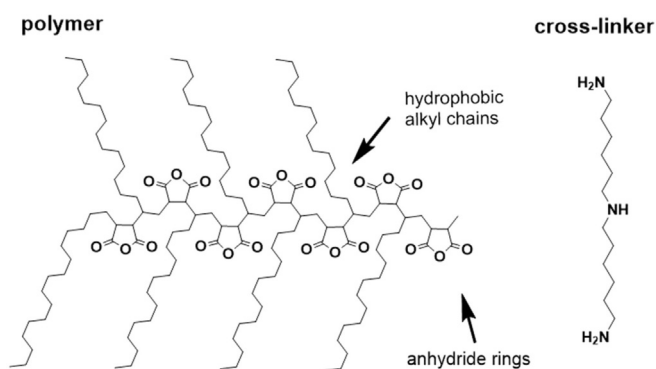## Shell-by-Shell (SbS)-Functionalization of Inorganic NPs: The Concept

Our SbS-functionalization concept was inspired by Pellegrino and co-workers,[9] who described a hybridization approach in which hydrophobically coated $CoPt_3$-, Au-, CdSe/ZnS-, and Fe_2O_3 nanocrystals were treated with amphiphilic polymers to switch their dispersibility from being soluble in nonpolar organic solvents to be being soluble in water (Figure 2).[9] As building blocks, poly(maleic anhydride alt-1-tetradecene) and bis(6-aminohexyl)amine (Figure 3) were used. Initially hydrophobic nanocrystals were treated with poly(maleic anhydride alt-1-tetradecene) in chloroform. After evaporation of the solvent, bis(6-aminohexyl)amine in chloroform was added to cross-link the polymer shell on the surface of the NP. After evaporation of the solvent, the NPs were dispersed in tris/borate/ethylene-diamine tetraacetate (EDTA) (TBE) buffer solution. After purification the NPs became dispersible in water. The polymer was wrapped around the first-shell functionalized hydrophobic nanocrystals. The corresponding self-assembly was guaranteed by hydrophobic interactions. The nonpolar tails of the amphiphilic polymer pointed inwards to the hydrophobic ligand shell and the polar headgroup pointed outwards to the water phase (Figure 2).

For the SbS-coating procedure, first covalent attachment of the first ligand shell has to be accomplished. Subsequently, the second ligand shell is introduced to complete the hierarchically ordered architecture. The wet-chemical assembly of the first ligand shell involves the combination of three components (Figure 1): a) the metal oxide NP itself, b) the organic ligand containing a suitable anchoring group, and c) a solvent, in which the NPs are dispersible and the organic ligands are soluble. Suitable anchoring groups for metal oxide NPs are silanes,
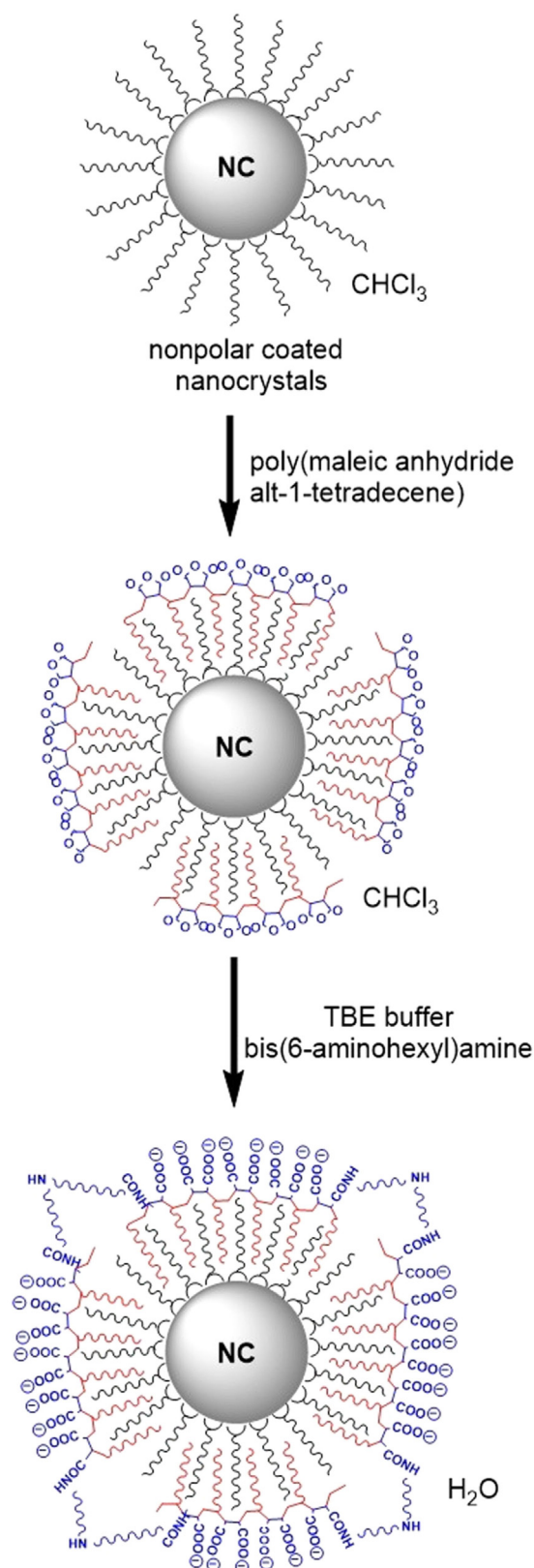
Figure 2. Bilayer coating procedure of nonpolar coated nanocrystals with an amphiphilic polymer shell, described by Pellegrino.[9]

phosphonates, carboxylates, catechols, alkenes/alkynes, amines, and others.[16] Phosphonic acids are the most efficient

Chemistry–A European Journal

Review
doi.org/10.1002/chem.202000195

**Chemistry
Europe**
European Chemical
Societies Publishing

Figure 3. Molecular building blocks for the bilayer coating procedure described by Pellegrino.[9]

binders to metal oxide NPs, because of a good compatibility with all classes of metal oxide surfaces and the formation of very stable binding to the metal oxide substrates.[17] A covalent attachment of the first ligand shell is not a prerequisite for the SbS-functionalization procedure, however it is imperative for the preparation of highly stable materials, since noncovalently attached first ligand shells can also be desorbed from the surface and can be washed-off from the surface successively. The chemistry of phosphonic acids and metal oxide surfaces is well established and has been extensively reviewed by Zuilhof[16] and there exists a wide range of publications dealing with the interaction of metal oxide surfaces with phosphonates.[18] The most common derivatives of phosphonates for wet-chemical metal oxide functionalization are phosphonic acids, dimethyl-phosphonates, diethyl-phosphonates and 1,1-bisphosphonic acids.[16] Phosphonates represent promising anchoring groups for hydroxylated surfaces, with an still increasing field of the so called phosphonate-based metal–organic frameworks (MOFs).[19] For the preparation of the first ligand shell on metal oxide NPs with phosphonates a widespread variety of solvents can be used. Water is specifically important, because of the limited solubility of phosphonates in non-aqueous solvents.[18a,d, 19a, 20] The choice of solvent is of high importance for the formation of stable and high-quality monolayers. A study has shown that solvents with low dielectric constants and therefore with insignificant interactions with the oxide surface, encourage more denser, and more stable monolayers.[20b] The dielectric constant of the solvent preferentially should be at about 4.[21] As opposed to this, high interacting solvents with high dielectric constants cause monolayers with lower quality,[20b] instead of stable monolayers, multilayers and aggregates could be formed. By using nonpolar solvents, the interaction between the phosphonic acid anchoring group and the hydrophilic substrate can be improved, and the generation of a fully covered monolayer is possible within a few minutes.[16] But not only the type of oxide is crucial for a stable bond formation, the reaction conditions such as temperature, pH value, concentration, and solvent media also play a key role in the functionalization process.[16] Two possible mechanisms for the chemisorption of phosphonates on metal oxide substrates are

known so far, depending on the acidity of the metal oxide surface, that could be Lewis acidic or poorly Lewis acidic.[15b,18c,19a,22] Phosphonates have three oxygen atoms available, consequently three binding modes results, these are mono-, bi-, and tridentate.[16] A further important reason for the usage of phosphonates is the relatively easy synthesis and purification, they are soluble in most organic solvents with easy conversion into phosphonic acids.[18c,19a,22,23] A further not negligible reason for the usage of phosphonates is that they are extremely stable against self-condensation reactions which can only be generated under high-temperature dehydrating conditions.[18c]

In comparison with other anchoring groups, such as carboxylates and catechols, the adsorption isotherm of phosphonic acids to the metal oxide substrate reveals most favorable binding properties.[17,24] Detailed knowledge about the necessary requirements for full surface coverage is an important prerequisite for further non-covalent functionalization. This data can be derived from X-ray photoelectron spectroscopy (XPS) measurements[25] or CHN elemental analysis.[26] In this article, we want to highlight a very efficient method for the determination of grafting densities, maximum monolayer grafting densities, absorption constants and negative free binding energy for first-shell functionalized NPs that was established by our group and is based on thermogravimetric analysis (TGA) measurements.[17,27] For this purpose, TiO$_2$ NPs were functionalized with different concentrations of hexadecylphosphonic acid, resulting in NP batches with different degrees of functionalization. Each NP batch was studied by TGA measurements. By increasing the amount of surfactant, the weight loss in the TGA curve increased (Figure 4). The measured weight loss (wt) of the TGA measurements, Avogadro constant, specific surface area (SSA) of the NP substrate, and molecular weight (MW) of the surfac-
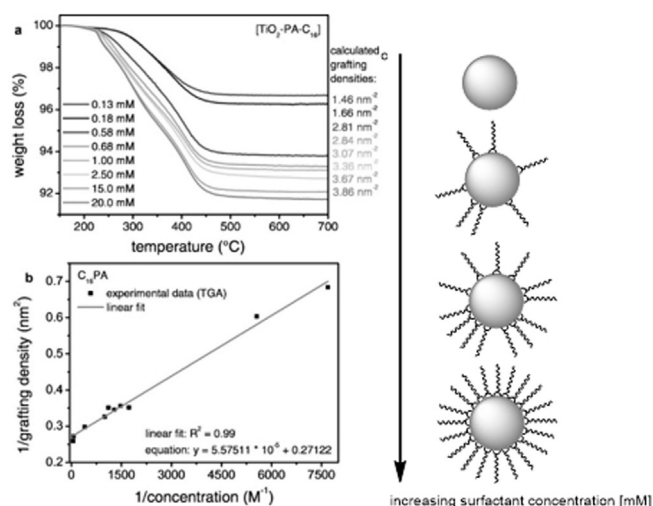
Figure 4. a) TGA weight-loss curves with the corresponding grafting densities of TiO$_2$ NPs with a fist ligand shell consisting of hexadecylphosphonic acid and b) plot of the reciprocal values of the calculated grafting densities;[17] c) schematic representation of NPs with different functionalization degree. Figure 4a, b reproduced from Ref. [17a]. Copyright 2016, Wiley-VCH.

Chemistry–A European Journal

Review
doi.org/10.1002/chem.202000195

**Chemistry
Europe**
European Chemical
Societies Publishing

tant were used to calculate the grafting densities, by using the following formula [Eq. (1)]:[17,28]

$$grafting\ density = \left(\frac{wt}{100 - wt}\right)\left(\frac{6.022*10^{23}}{MW*SSA}\right)$$

By plotting the reciprocal values of grafting densities (TGA) versus reciprocal surfactant concentrations that were used for the NP functionalization, a linear fit could be applied (Figure 4b). From the intercept of the linear fit, the maximum monolayer grafting density (Θ_{max}) could be determined. For the determination of the adsorption constant (K_{ads}) for ligand adsorption the following formula with given values from the linear fit was employed [Eq. (2)–(4)]:

$$y = a*x + b\Theta_{max} = \frac{1}{b} \tag{2}$$

$$K_{ads} = \frac{b}{a} \tag{3}$$

$$\Delta G = -R*T*lnK_{ads} \tag{4}$$

The maximum grafting density was the reciprocal value of the intercept of the linear fit 1/grafting density versus 1/concentration. The adsorption constant was determined from the intercept and the slope. This allows for the calculation of the adsorption constant (K_{ads}) and, hence, the determination of the free enthalpy ΔG.

For TiO$_2$ (anatase) NPs with a specific surface area of 46 m^2 g^{-1} and an average diameter of 34 nm, as determined by Brunauer–Emmett–Teller (BET) measurements, a maximum monolayer grafting density of 3.7 nm was determined for hexadecylphosphonic acid functionalized NPs.[17] This value is in good agreement with a precedent reported by Halik, where an alumina surface was treated with n-octadecylphosphonic acid leading to a packing density of 4.6 molecules per nm^2, as determined by XPS analysis.[25a] The absorption constant was calculated to be $K_{ads} = 4865$ M^{-1} with a negative free binding energy of 21.0 kJ mol^{-1}, which is also in good agreement with formerly studied comparable systems from Peukert and Segets.[29]

The dispersibility of such fist-shell functionalized NPs depends on the tail of the phosphonic acid ligand. If the phosphonic acid includes a lipophilic moiety, the NPs become dispersible in nonpolar solvents, like toluene or hexane. In the case of polar termini, the corresponding NPs become dispersible in polar solvents and by employing a fluorinated phosphonic acid, the particles are well dispersible in fluorinated solvents. The building block for the second ligand shell consists of an amphiphile with a moiety that has a polarity equivalent to the terminus of the phosphonic acid terminus and a moiety with a polarity orthogonal to the phosphonic acid terminus. This can be either a lipophilic, hydrophilic, or fluorophilic chain. The assembly of the second shell is driven by solvophobic interactions. The corresponding orthogonal parts of the second shell molecules are directed towards the dispersion medium. Thus, the dispersibility of the NPs during the SbS-functionalization process switches two times. The SbS-coated

NPs contain a sterically demanding ligand shell, which brings-up enhanced dispersibility and stability in compatible solvents. An example of such a SbS-architecture is sketched in Figure 1. The first ligand shell of the metal oxide NP is provided by hexadecylphosphonic acid. The anchoring phosphonic acid binds covalently to the metal oxide surface and the lipophilic moiety point outwards. These functionalized NPs are well dispersible in lipophilic/nonpolar solvents, like toluene. The second ligand shell is comprised of sodium dodecylbenzene sulfonate (SDBS). This is associated with a switch of dispersibility from toluene to water. The entire SbS-architectures are very stable in aqueous dispersion and exhibit a negative zeta potential, due to the negatively charged headgroups of SDBS.[30] In Figure 5 a series of amphiphilic building blocks 1–7 that
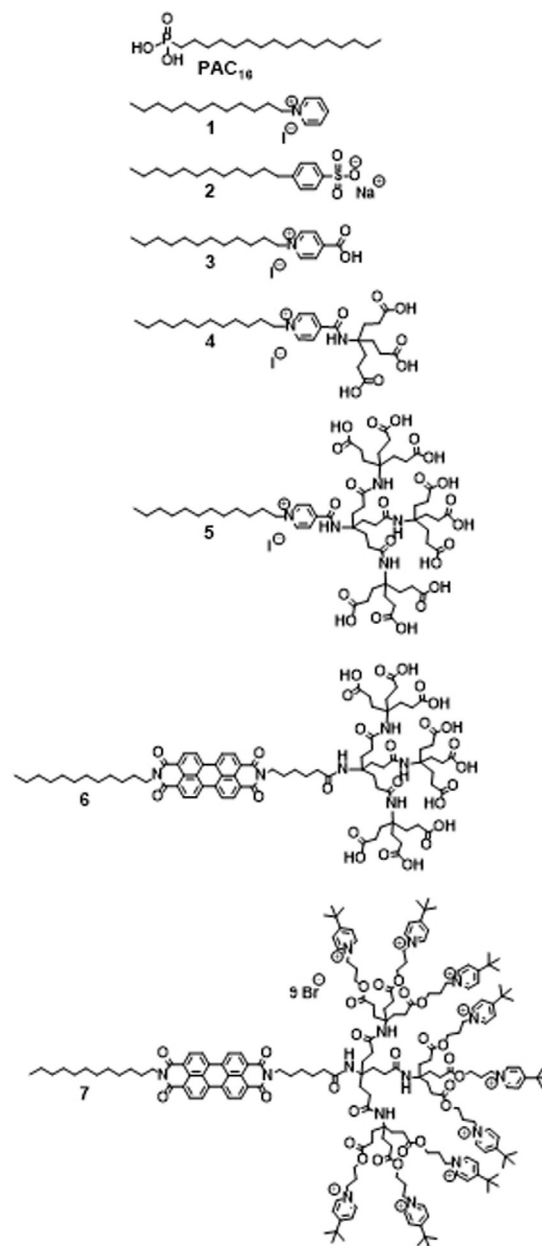
Figure 5. Amphiphilic building blocks used for the SbS-coating of TiO$_2$ NPs.[1a]

have been used for the SbS-functionalization of TiO$_2$ (anatase) NPs with an average diameter of 34 nm are listed.

After the incorporation of the amphiphiles **1–7**, the corresponding SbS-architectures were characterized by zeta potential and dynamic light scattering (DLS) measurements (Table 1, Figure 6). With surfactant **1** as the second-shell ligand, the zeta potential becomes positive due to the positively charged head group. Alternatively, using surfactant **2** leads to a negative zeta potential, as expected for the negatively charged outer shell ligands. Switchable zeta potentials were found for the zwitterionic systems [TiO$_2$-(PAC$_{16}$)]A**3**, [TiO$_2$-(PAC$_{16}$)]A**4**, and [TiO$_2$-(PAC$_{16}$)]A**5** in pH-dependent measurements.[1a] [TiO$_2$-(PA C$_{16}$)]A**3** has a zeta potential of about −14.3 mV at pH 7.2. At neutral pH, the carboxy group is deprotonated, leading to a negative zeta potential. Going to pH 10 shifts the potential to −15.6 mV, and at an acidic pH of 5 the zeta potential shifts to +9.4 mV. The zwitterionic dendritic amphiphile **4** and **5** contain a ratio of terminal carboxylic acids to inner pyridinium groups of 3:1 and 9:1 which cause negative zeta potentials, even under slightly acidic conditions (Table 1).[1a] Due to the 9 carboxylic head groups of amphiphile **6**, negative zeta potentials were measured. On the other hand, for amphiphile **7** with nine pyridinium-bromide headgroups, positive zeta potentials were found.

We have further characterized the SbS-functionalized NPs in water by DLS measurements (Figure 6). The hydrodynamic diameters of the colloidal NPs depend on the functionalization degree, the bulkiness of the amphiphile and its polar head group. First-shell functionalized NPs with missing electrostatic stabilization have the largest hydrodynamic diameter in water and tend to agglomerate. The naked TiO$_2$ NPs have the smallest hydrodynamic diameter of around 50 nm, followed by the SbS-functionalized NPs with hydrodynamic diameters measured in a size range from 60 to 150 nm.[1a]

Three-Phase Systems

A common method for the characterization of the surface properties of NPs, like surface wetting, is the measurement of static contact angles (SCAs; Figure 7). Is a liquid in contact with a solid with existing equilibrium in between, the Young equation can be applied [Eq. (5)]:[31]

$$\cos\theta_Y = (\sigma_s - \sigma_{sl})/\sigma_l \qquad (5)$$

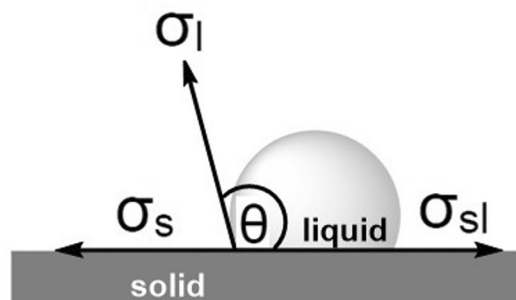in which σ_s: surface energy of the solid; σ_{sl}: interfacial tension of the solid–liquid phase interface; σ_l: surface tension of the liquid (like diiodomethane,[32] water.[32b] *n*-hexadecane[33]); θ_Y: contact angle ($\theta_{Y\,small}\rightarrow$good wetting; $\theta_{Y\,big}\rightarrow$poor wetting)[34] For $\sigma_s > \sigma_{sl}$: $0° < \theta < 90°$ and $\sigma_{sl} > \sigma_s$: $90° < \theta < 180°$.

The surface tunability and wettability was intensively investigated by Marder, who modified indium-tin oxide (ITO) electrodes with different types of phosphonic acids, which resulted in various surface energies.[25c] Therefore, activated ITO slides were immersed horizontally in a 1 mM ethanol solution of the respective phosphonic acid for 3.5 h. Further workup including washing of the slides to remove multilayer material as well as backing the slides in an oven for complementation of the chemical bindings, followed. Figure 8 shows bar graphs of indium-tin oxide electrodes treated with the phosphonic acids *n*-hexylphosphonic acid (HPA), *n*-octadecylphosphonic acid (ODPA), 3,3,4,4,5,5,6,6,7,7,8,8,8-tridecafluorooctyl phosphonic acid (FHOPA), pentafluorobenzyl phosphonic acid (PFBPA), and tetrafluorobenzyl-1,4-diphosphonic acid (TFBdiPA) as well as reference measurements of ITO electrodes after detergent/sol-
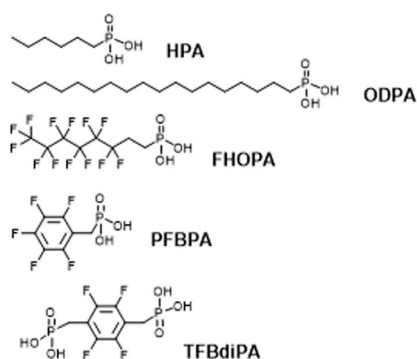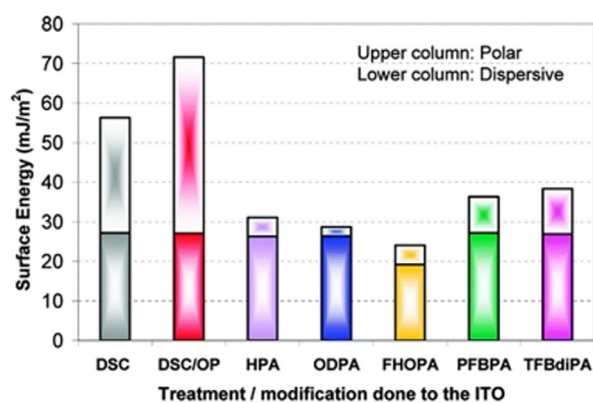
Table 1. PH-dependent zeta-potential measurements of [TiO$_2$-(PAC$_{16}$)]A**1–7** determined in phosphate buffer (7.2), acetate buffer (5.1) and borax/NaOH buffer (10.0).[1a]

[TiO$_2$-(PAC$_{16}$)]A	pH	Zeta potential [mV]	Standard deviation
1	7.2	+17.6	±0.7
2	7.2	−40.6	±0.9
3	5.1	+9.4	±1.6
	7.2	−14.3	±1.4
	10.0	−15.6	±0.4
4	5.1	−12.8	±1.1
	7.2	−31.6	±1.5
	10.0	−36.0	±1.6
5	5.1	−13.0	±3.2
	7.2	−29.9	±0.6
	10.0	−36.1	±1.3
6	7.2	−41.9	±0.8
7	7.2	+40.9	±1.1
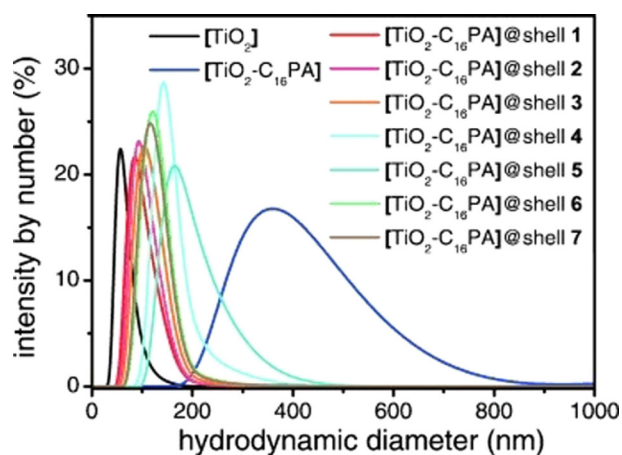
Figure 6. DLS measurements of TiO$_2$, TiO$_2$-(PAC$_{16}$), and [TiO$_2$-(PAC$_{16}$)]A**1–7** NPs determined in water. Reproduced from Ref. [1a]. Copyright 2015, Wiley-VCH.

Figure 7. Schematic representation of the static contact angle and wetting.

Chemistry–A European Journal

Review

doi.org/10.1002/chem.202000195

Chemistry
Europe
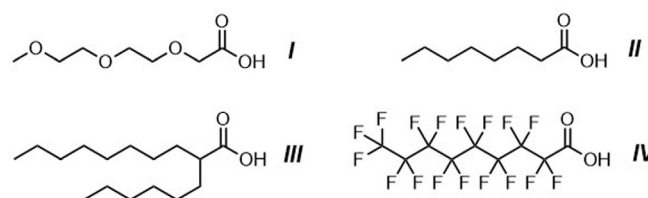European Chemical
Societies Publishing

Figure 8. Bar graph with surface energies of indium-tin oxide electrodes treated with DSC, DSC/OP, or with various phosphonic acids (HPA, ODPA, FHOPA, PFBPA, or TFBdiPA). Reproduced from Ref. [25c]. Copyright 2008, American Chemical Society.

Figure 9. Carboxylic acids used for the functionalization of aluminum oxide NPs with different substituents that bring along polarity modifications to the NP surface.[36]

vent cleaning (DSC) and DSC in combination with treatment of the surface with oxygen-plasma (OP). The ITO electrodes without phosphonic acid functionalization show high surface energies compared with the phosphonic acid treated surfaces. The higher the surface energies, the more polar was the surface with low water contact angles. The high polarity of ITO substrates is characteristic and after treatment with oxygen-plasma, the surface has a hydroxylated surface which brings up an increased polarity on the surface compared to the surface, that was just treated with DSC. Implementation of the ITO substrates with phosphonic acids leads to decreased surface energies. The system with the lowest surface energy was with FHOPA, the outstanding fluorocarbons pull-down the surface energy enormous, compared to systems that have an increased presence of hydrocarbon substituents/fragments in its chemical structure that will be in contact with the probe liquids.[15b, 35]

These investigations of the surface properties of phosphonic acid functionalized indium-tin oxide electrodes were also transferred to aluminum oxide NPs.[36] The surface properties were varied from highly hydrophobic to highly hydrophilic by using carboxylic acids bearing substituents with diverse polarity (Figure 9).

After the treatment of aluminum oxide NPs with 2-[2-(2-me-thoxyethoxy)ethoxy]acetic acid (MEEA, *I*), the particle surface become highly hydrophilic with a surface energy of 80.7 mN m^{-1}. By functionalizing particles with octanoic acid (*II*),

a hydrophobic surface with a surface energy of 53.5 mN m^{-1} was created. The surface energy could be decreased to 48.5 mN m^{-1} by implying a carboxylic acid with a branched hydrocarbon chain, namely 2-hexyldecanoic acid (*III*). As expected, a carboxylic acid with a fluorinated tail, namely 9*H*-hexadecafluorononanoic acid (*IV*), generated the surface with the lowest surface energy of 6.1 mN m^{-1} with superhydrophobic characteristics.[36]

In another study, aluminum oxide NPs were functionalized with phosphonic acids bearing substituents with opposite polarities and mixtures of them in different ratios (Figure 10).
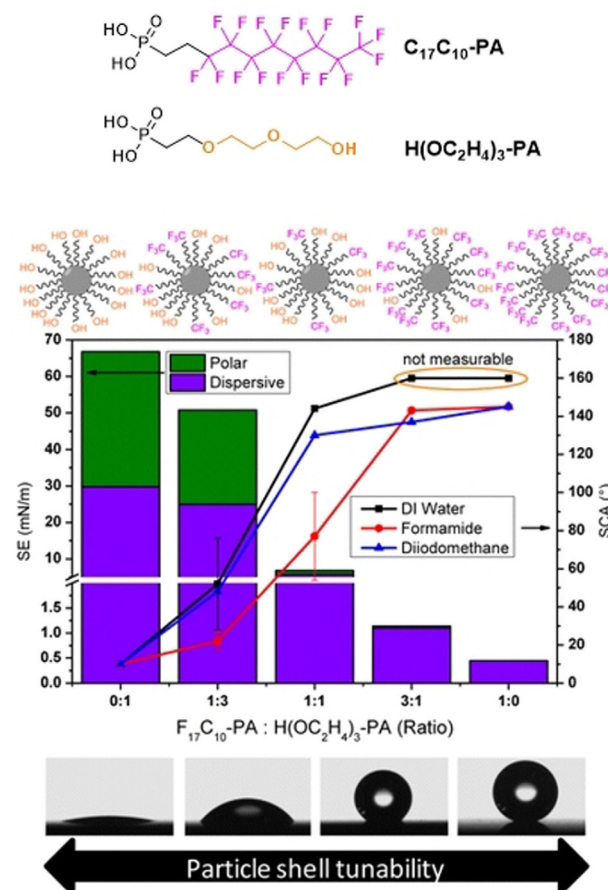
Figure 10. Tunability of surface energies of aluminum oxide NPs functionalized with phosphonic acids bearing substituents with opposite polarity and mixtures of it. Reproduced from Ref. [15a]. Copyright 2014, American Chemical Society.

Functionalized particles with 3,3,4,4,5,5,6,6,7,7,8,8,9,9, 10,10,10-heptadecafluorodecylphosphonic acid ($F_{17}C_{10}$-PA) have a total surface energy of 0.45 mN m^{-1} and were dispersible in fluorocarbons. In contrast, particles functionalized with (2-(2-[2-hydroxy-ethoxy]-ethoxy)-ethyl) phosphonic acid [H-(OC$_2$H$_4$)$_3$-PA] have a total surface energy of 67 mN m^{-1} and were dispersible in water. The surface energies are due to hydrophobicity of $F_{17}C_{10}$-PA functionalized surfaces and hydrophilicity of [H-(OC$_2$H$_4$)$_3$-PA] functionalized surfaces. By continuous decreasing the amount of $F_{17}C_{10}$-PA and increasing amount of [H-(OC$_2$H$_4$)$_3$-PA], a stepwise tunability of NP surface energies from super-hydrophobic to super-hydrophilic was presented for the first time.[15a]

In a next step of complexity, a SbS-concept was introduced, in which the surface properties of titanium dioxide NPs were switched between lipophilic, hydrophilic, and fluorophilic with respective dispersibility in hydrocarbons, water, and fluorocarbons. Initially, TiO$_2$ (anatase) NPs were functionalized with hexadecylphosphonic acid (1, PA-HC), (2-(2-(2-hydroxyethoxy)-ethoxy)ethyl)phosphonic acid (2, PA-PEG), or (3,3,4,4,5,5, 6,6,7,7,8,8,9,9,10,10,10-heptadecafluorodecyl)phosphonic acid (3, PA-FC) and in a further step, the first-shell functionalized NPs were treated with the corresponding amphiphiles (4,HC-PEG/ 5, HC-FC/ 6, FC-PEG) (Figure 11).

The NP hybrids TiO$_2$-(PA-HC), that were functionalized with HC-PA have a lipophilic surface with a surface energy of around 35 mN m^{-1}. These particles are dispersible in hydrocarbons. Subsequently, an attachment of a second shell followed. By applying amphiphile 4 as a second shell building block, resulting in [TiO$_2$-(PA-HC)]A^4 hybrids, the dispersibility of the NPs was switched from hydrocarbons to water. The polar tail of amphiphile 4 points outwards and creates dispersibility in water. These NPs have a surface energy of around 65 mN m^{-1}. By implementing amphiphile 5 as a second shell building block with TiO$_2$-(PA-HC), resulting in [TiO$_2$-(PA-HC)]A^5, the dispersibility behavior switched from hydrocarbons to fluorocarbons through fluorophobic interactions of the hydrocarbon tail of amphiphile 5 that was incorporated into the first ligand

shell. The fluorocarbon tail points outwards and causes dispersibility in fluorocarbons with NP-surface energies of around 10 mN m^{-1}. Titanium dioxide NPs functionalized with PEG-PA, namely TiO$_2$-(PA-PEG), exhibit a polar surface with dispersibility in water and a surface energy of around 80 mN m^{-1}. By complementing the SbS-architecture with amphiphile 4, the dispersibility behavior of the [TiO$_2$-(PA-PEG)]A^4 NPs changes from water to hydrocarbons, driven by lipophobic interactions. Thereby the surface energy decreased from 80 mN m^{-1} to around 25 mN m^{-1}. The surface energy could be further lowered down to 15 mN m^{-1} by employing amphiphile 6 as a second-shell building block. The [TiO$_2$-(PA-PEG)]A^6 NPs contain a fluorophilic surface with pronounced dispersibility in fluorocarbons. The tunability from fluorinated surfaces to hydrocarbon and polar surfaces was also studied. Titanium dioxide NPs, that were implemented with FC-PA, TiO$_2$-(PA-FC), have a fluorophilic surface with dispersibility in fluorocarbons and a surface energy of around 8 mN m^{-1}. By attaching amphiphile 5 leading to [TiO$_2$-(PA-FC)]A^5 the dispersibility changes to hydrocarbons with an increased surface energy of 25 mN m^{-1}. The surface energy was further increased by addition of amphiphile 6, resulting in [TiO$_2$-(PA-FC)]A^6 NPs that are dispersible in water. With these investigations, a now supramolecular concept of switchable dispersibility of NPs between hydrocarbons, water, and fluorocarbons was introduced (Figure 12, Table 2).[1b]
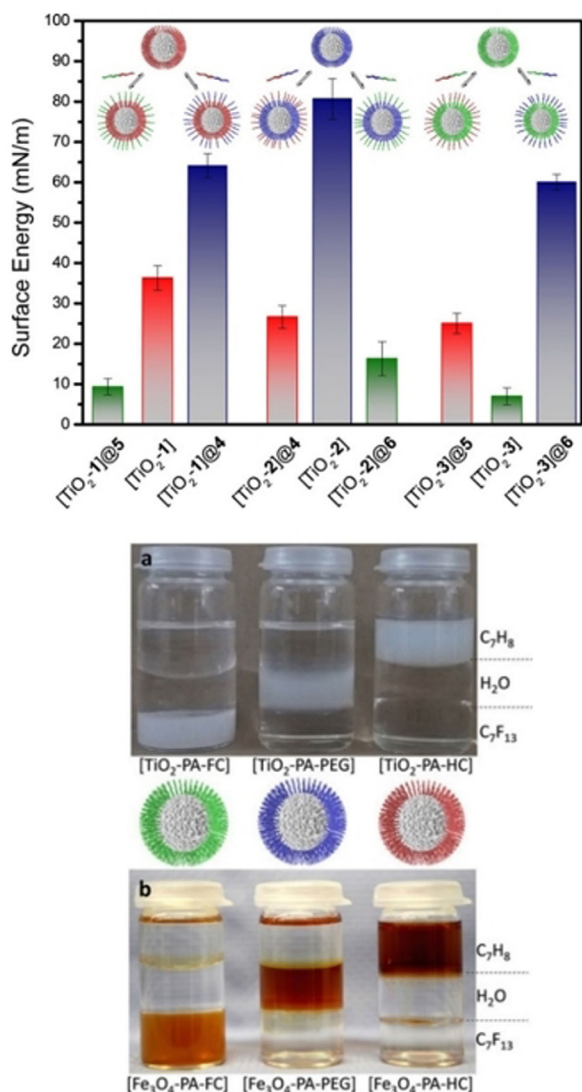
Optoelectronic Interactions in SbS-Functionalized NPs

The SbS-functionalization approach was also used to tune the optical and electronical properties of NPs. For this purpose Al$_2$O$_3$ NPs ($<$50 nm in DLS measurements) were functionalized with a pyrene-phosphonic acid, namely (12-(4-(pyren-1-yl)-1H-1,2,3-triazol-1-yl)dodecyl)phosphonic acid (PA-Py), together with matrix (or spacing) phosphonic acids hexadecylphosphonic acid (PA-CH$_3$) or (12,12,13,13,14,14,15,15,16,16,17,17,18,18,18-pentadecafluorooctadecyl)phosphonic acid (PA-CF$_3$) (Figure 13). For the functionalization, a mixture of 10% optical active PA-Py and 90% of the matrix phosphonic acids was used, leading to Al$_2$O$_3$-(PA-Py$^{10\%}$ PA-CH$_3$$^{90\%}$) and Al$_2O_3$-(PA-Py$^{10\%}$ PA-CF$_3$$^{90\%}$) nanocomposites.[1d] Depending on the matrix phosphonic acid that was used, different fluorescence properties of the pyrene-unit with either predominant monomer or excimer band were observed.[37] By using the hexadecylphosphonic acid as a matrix phosphonic acid, a monomeric as well as excimeric fluorescence band was observed in a ratio of approximately 1:1. By using the fluorinated component, a strong monomer band with negligible excimer band was formed. Reason for that phenomenon was, that the fluorocarbons are more rigid than the hydrocarbons[1d, 38] and were thus able to seperate the pyrene units more efficient onto the NP surface than the hydrocarbons. In a next step to further modify the optical properties of the pyrene unit, amphiphiles were added as second-shell building blocks (Figure 14). By starting with the Al$_2$O$_3$-(PA-Py$^{10\%}$ PA-
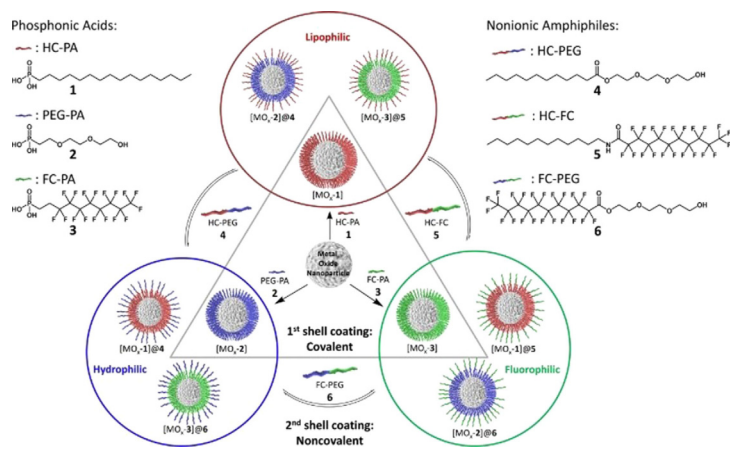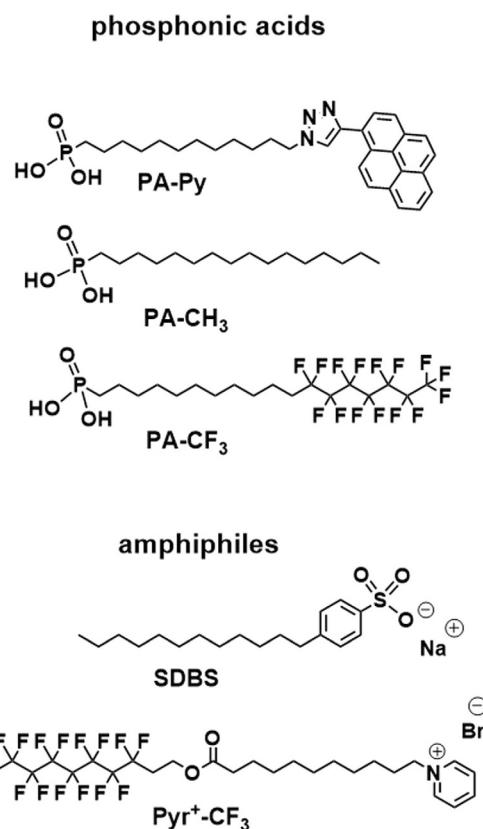

Figure 11. Triangle of SbS-functionalized metal oxide NPs with switchable surface properties resulting in lipophilic, hydrophilic, and fluorophilic surfaces. Reproduced from Ref. [1b]. Copyright 2018, The Authors.

Chemistry–A European Journal

Review

doi.org/10.1002/chem.202000195

Chemistry
Europe
European Chemical
Societies Publishing

Figure 12. Bar graphs with surface energies measured for SbS-functionalized titanium dioxide NPs and an illustration of titanium dioxide (TiO₂) and iron oxide (Fe₃O₄) NPs with either fluorophilic, lipophilic, and polar surfaces and respective dispersibility in fluorocarbons, hydrocarbons, and water. Reproduced from Ref. [1b]. Copyright 2018, The Authors.

Figure 13. Molecular building blocks for the tunability of optical properties of SbS-functionalized NPs.[1d]

CH₃⁹⁰ %) nanocomposites, SDBS was used to generate the second shell. The arrangement of SDBS around first-shell functionalized NPs caused a strong decrease of the excimer band with a concomitant increase of the monomer band, as shown in Figure 20. This was a successful proof of concept, for the
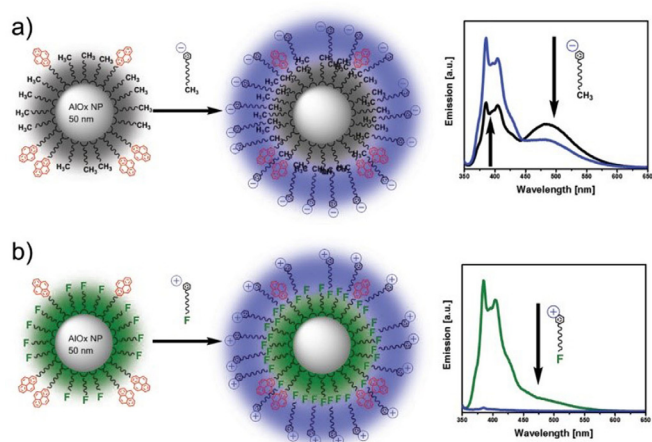
fact that the second shell is incorporated between the first ligand shell and separate the pyrene excimers onto the NP surface. By studying the optical properties of the Al₂O₃-(PA-Py¹⁰ % PA-CF₃⁹⁰ %) nanocomposites, it was demonstrated, that the fluorescence of the NPs caused by the pyrene chromophore can be switched on and off. By applying 1-(11-((3,3,4,4,5,5,6,6,7,7,8,8,9,9,10,10,10-heptadecafluorodecyl)oxy)-11-oxoundecyl)pyridin-1-ium bromide (Pyr⁺-CF₃) as a second shell building block, the pyrene-fluorescence was turned off, as shown in Figure 20. Pyridinium is known to quench the fluorescence of alternant polycyclic aromatic hydrocarbons in water or acetonitrile and can thus be easily used to modify the optical properties of pyrene.[39] On the other side, by removing the second shell (Pyr⁺-CF₃) from the Al₂O₃-(PA-Py¹⁰ % PA-CF₃⁹⁰ %) NPs through washing, the fluorescence could be turned on again.

Table 2. Overview of phosphonic acid and amphiphile combinations for the *SbS*-functionalization of metal oxide NPs with solvent specification and information about the solvophobic effect as a driving force for the self-assembly structure of amphiphiles around first-shell functionalized NPs.
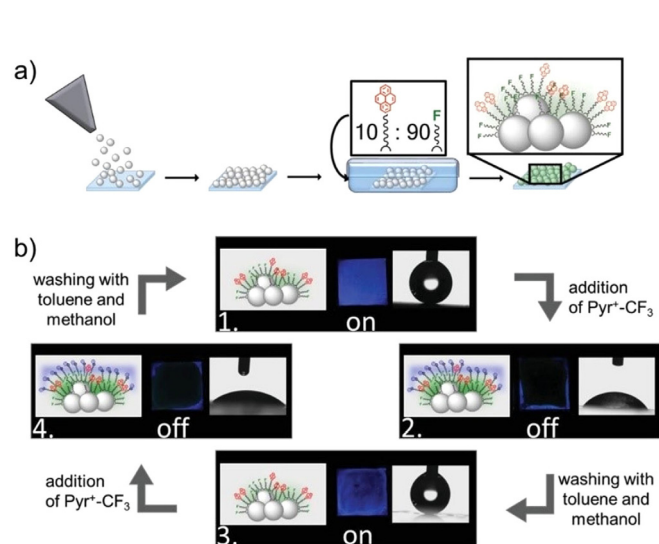
1st shell	2nd shell	Solvent	Solvophobic effect
hydrocarbon (1)	hydrocarbon-polar (4)	H₂O	hydrophobic
	hydrocarbon-fluorocarbon (5)	fluorocarbon	fluorophobic
polar (2)	polar-hydrocarbon (4)	hydrocarbon	lipophobic
	polar-fluorocarbon (6)	fluorocarbon	fluorophobic
fluorocarbon (3)	fluorocarbon-polar (6)	H₂O	hydrophobic
	fluorocarbon-hydrocarbon (5)	hydrocarbon	lipophobic

Chemistry–A European Journal

Review
doi.org/10.1002/chem.202000195

Chemistry Europe
European Chemical
Societies Publishing

Figure 14. SbS-functionalized NPs [Al$_2$O$_3$-(PA-Py$^{10\%}$ PA-CH$_3$$^{90\%}$)]SDBS and [Al$_2O_3$-(PA-Py$^{10\%}$ PA-CF$_3$$^{90\%}$)]Pyr$^+$-CF$_3$ with corresponding fluorescence measurements. Reproduced from Ref. [1d]. Copyright 2019, Wiley-VCH.

The hydrodynamic diameters of both *SbS*-functionalized Al$_2$O$_3$-(PA-Py$^{10\%}$ PA-CH$_3$$^{90\%}$) nanocomposites were in the same size range, that is 154±7 nm for the system with SDBS and 143±8 nm for the system with Pyr$^+$-CF$_3$ attached as a second ligand shell.[1d]

The concept of turning on and off the fluorescence properties of Al$_2$O$_3$-(PA-Py$^{10\%}$ PA-CF$_3$$^{90\%}$) NPs with Pyr$^+$-CF$_3$, was also transferred to nano-porous flat surfaces (Figure 15).[1d] Al$_2$O$_3$ NPs were sintered onto a glass slide and backed in an oven. Subsequently, the glass slide with the Al$_2$O$_3$ NP surface was dipped in a phosphonic acid solution in a ratio of 10% PA-Py and 90% PA-CF$_3$ in toluene/methanol (1:1), to build up a self-assembled monolayer (SAM) onto the NP surface on the glass slide with the same composition of phosphonic acids as pres-
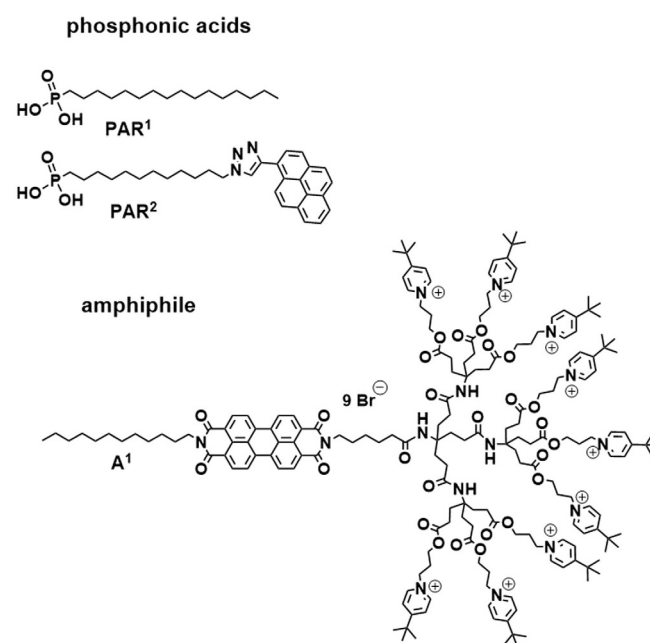
ent in the NP dispersions. By dipping them in an aqueous Pyr$^+$-CF$_3$ solution, the fluorescence was turned off. After washing the slides with toluene and methanol, the fluorescence turned on again. This cycle can be performed many times, until the sintered NPs starts to break away from the glass slide.
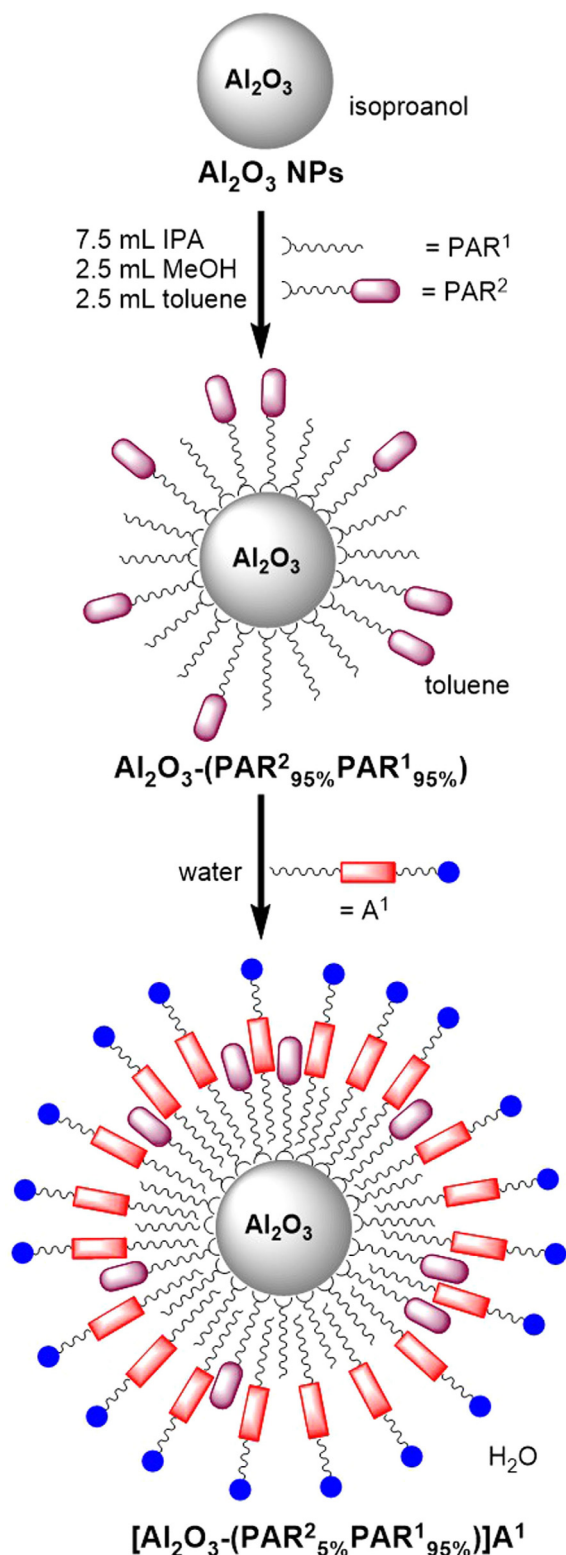
Also electronic communication between first and second shell building blocks with different electron demand (Figure 16) has been investigated.[11] In detail, electronically inert Al$_2$O$_3$ NPs were functionalized with 95% PAR^1 and 5% PAR^2, resulting in Al$_2$O$_3$-(PAR^2$_{5\%}$PAR^1$_{95\%}$) NPs. The NPs were further modified with an amphiphilic perylenediimide (PDI) building block carrying a positively charged pyridinium bromide headgroup (A^1) as a second shell building block, resulting in [Al$_2$O$_3$-(PAR^2$_{5\%}$PAR^1$_{95\%}$)]A^1 NP hybrids (Figure 17).

This highly hierarchical structure contains the pyrene unit of PAR^2 as an electron donor in the first ligand shell and the perylene core[40]/pyridinium[41] substituents of the polar headgroup of amphiphile A^1 as electron acceptor functionalities in the second ligand shell. Based on these architectures systematic studies have been carried out, where first-shell functionalized Al$_2$O$_3$-(PAR^2$_{5\%}$PAR^1$_{95\%}$) NPs were titrated with second-shell functionalized [Al$_2$O$_3$-(PAR^2$_{5\%}$PAR^1$_{95\%}$)]A^1 NPs to measure the optical properties of the pyrene unit of Al$_2$O$_3$-(PAR^2$_{5\%}$PAR^1$_{95\%}$) NPs in dependence on the amphiphile concentration A^1 (Figure 18). The first-shell functionalized Al$_2$O$_3$-(PAR^2$_{5\%}$PAR^1$_{95\%}$) NPs reveal of a pronounced fluorescence signal with a strong monomer band and a weak excimer band after irradiation of light with a wavelength of $\lambda_{ext}=340$ nm. During titration of amphiphile A^1 to first-shell functionalized NPs, the typical absorption signals of the PDI core of A^1 increased with its strongest absorption band at $\lambda_{max}=533$ nm. Fluorescence measurements showed that the PDI core emits with a fluorescence maximum at $\lambda_{max}=$

Figure 15. SbS-NP functionalization onto glass slides, a) sintering of Al$_2$O$_3$ NPs onto the glass slide and immersion into a phosphonic acid mixture solution of 10% PA-Py and 90% PA-CF$_3$ for the SAM formation, b) attachment of Pyr$^+$-CF$_3$ as a second shell with presentation of the fluorescence on and off switching of the pyrene unit. Reproduced from Ref. [1d]. Copyright 2019, Wiley-VCH.
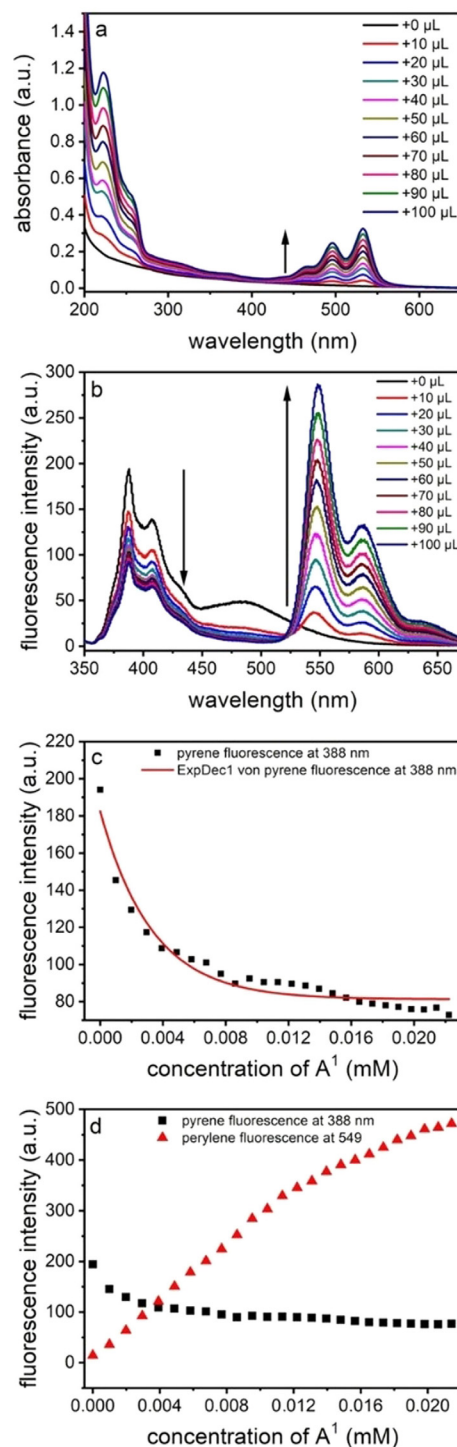

Figure 16. Molecular building blocks for the tunability of electronical properties of *SbS*-functionalized NPs.[11]

Chemistry–A European Journal

Review

doi.org/10.1002/chem.202000195

Chemistry Europe
European Chemical
Societies Publishing

Figure 17. Schematic representation of the *SbS*-functionalization of Al_2O_3 NPs resulting in Al_2O_3-(PAR$^2_{5\%}$PAR$^1_{95\%}$) and [Al_2O_3-(PAR$^2_{5\%}$PAR$^1_{95\%}$)]A^1 NP hybrids. Adapted from Ref. [11]. Copyright 2019, Wiley-VCH.

Figure 18. Optical measurements of Al_2O_3-(PAR$^2_{5\%}$PAR$^1_{95\%}$) NPs in dependence on the titrated concentration of A^1. Reproduced from Ref. [11]. Copyright 2019, Wiley-VCH.

550 nm. At the same time, the fluorescence of the pyrene unit decreased during titration with A^1, as a successful proof for the electronic communication between the electron rich pyrene

unit and the electron poor perylenediimide/pyridinium functionalities. After the first addition of A^1 leading to a concentration of 0.001 mм, the excimer band fully disappeared and also the quenching of the monomer band was most pronounced.[37c,42] Further titration steps of A^1 caused a decreased quenching of the pyrene monomer fluorescence compared

Chemistry–A European Journal

Review
doi.org/10.1002/chem.202000195

Chemistry Europe
European Chemical
Societies Publishing

with the first quenching step. The quenching of the monomer emission of the pyrene unit of Al_2O_3-$(PAR^2_{5\%}PAR^1_{95\%})$ NPs with A^1 follows an exponential decay. Reason for the exponential decay is that during the titration, a fully covered second shell of A^1 was built-up among first-shell functionalized NPs. When the coverage of the second shell with amphiphile was nearly complete, the excess of A^1 causes a reduced impact to the electronical communication with the first-shell functionalized Al_2O_3-$(PAR^2_{5\%}PAR^1_{95\%})$ NPs leading to less pronounced quenching of the pyrene unit. The concept of the formation of $[Al_2O_3$-$(PAR^2_{5\%}PAR^1_{95\%})]A^1$ NPs with tunable electronic properties within the ligand shells represents an attractive model for more complex architectures to be investigated in the future.

Applications of SbS-functionalized NPs

Water-cleaning materials

Adsorption and encapsulation of nonpolar molecules through tailored NP hybrids

Oil disasters in the seas or the accumulation of pesticides like polychlorinated biphenyls (PCBs) in the groundwater poses long lasting effects on the environment with a major threat for the aquatic life and the food chain.[43] In recent years, magnetic nanomaterials have attracted interest as water-cleaning materials because they combine a high active surface area, versatile functionalization, easy synthesis and facile removal by utilization of the materials intrinsic magnetic properties.[44] Therefore, a contamination of the treated water sources with detergent chemicals can be avoided. In this section we want to highlight several promising approaches towards the utilization of tailor-made magnetic NPs for the adsorption and removal of nonpolar water contaminants. Recent work by Halik and our group demonstrated the preparation of smart surfaces through the deposition of first ligand-shells on metal oxide NPs.[1b, 15a, 17] Using NPs with a lipophilic/hydrophobic first ligand-shell, affinity for the adsorption of hydrophobic molecules in water can be reached. Through utilization of the intrinsic magnetic properties of first-shell functionalized Fe_3O_4 NPs, Halik demonstrated the adsorption of hydrocarbons in water, followed by magnetic collection of the NPs (Figure 19).[14b]

Additionally, molecular dynamics investigations of the water–oil segregation displayed various segregation energies depending on the molecular structure of the oil phase (Figure 20). Thus, particularly strong driving forces for segregation were measured in case of *n*-alkanes, followed by branched alkanes, whereas aromatic molecules displayed lower segregation energies. Upon magnetic removal of the previously formed NP–oil phase from water, the binding of the oil phase is no longer supported by hydrophobic interactions and solely depending on London forces. The molecular dynamics (MD) simulations revealed the strongest interactions in case of aromatic molecules and thus a compensation of the lower segregation energies by stronger binding to the NPs first ligand-shell upon magnetic extraction from the water phase.[14b] The extraction rates (ER) data for Fe_3O_4-(PAC_{16}) with an average volumetric ER_{vol} of 10.6 times the sorbent volume and a gravi-
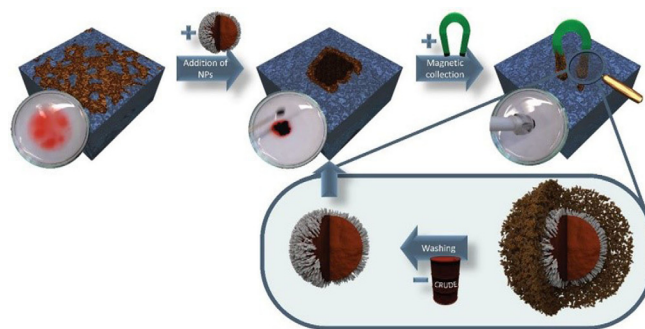
Figure 19. Schematic of the extraction procedure of HCs from water with the Fe_3O_4-(PAC_{16}). The NPs are added to oil in water and allowed to soak the oil. Then, the NPs are collected with a magnetic bar and washed in suitable solvent. After this, the NPs are recollected by the magnetic bar and added to the oil-water mixture for another extraction cycle. This process can be repeated. Reproduced from Ref. [14b]. Copyright 2019, Wiley-VCH.
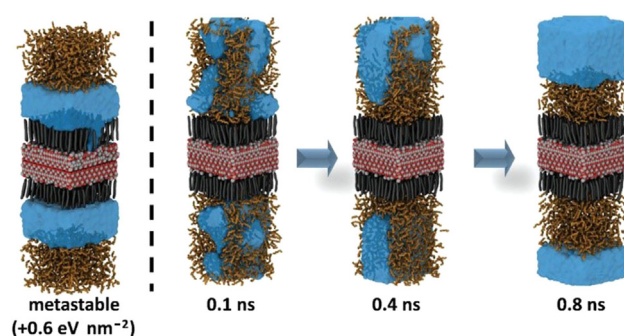
Figure 20. Snapshots from molecular dynamics simulations of heptane/water/ligand-magnetite sandwich systems with 3D periodic boundary conditions. The model includes 7402 water molecules (transparent blue), 1225 heptane molecules (brown sticks), and the magnetite-ligand (Fe: gray; O: red; alkyl chains: dark gray) slab. Left: Preparation of oil-water-ligand films leads to metastable sandwiches, which were characterized from 2 ns simulation runs at ambient conditions. Right: relaxation of a randomly prepared oil-water mixture to water-oil-ligand films. Reproduced from Ref. [14b]. Copyright 2019, Wiley-VCH.
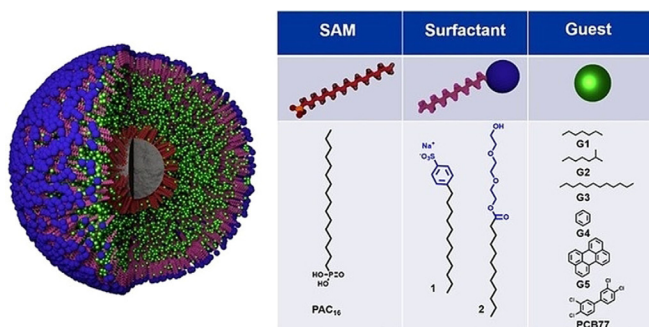
metric ER_{mass} of 2.5, show the competitiveness with other sorbent materials like foams and polymerically coated NPs. Uniquely compared to the other materials, the ER of Fe_3O_4-(PAC_{16}) stayed constant over multiple cycles of oil adsorption followed by magnetic extraction from the water source. This outstanding stability is a result of the strong surface attachment of the phosphonic acid headgroup and results in a constantly hydrophobic and super-oleophilic NP shell, suitable for the reversible noncovalent binding of hydrocarbons.

Encapsulation and phase separation of nonpolar molecules

Another approach introduced by our group relies on the utilization of the SbS-coating concept described earlier in this review.[1a, c] After the formation of a first ligand-shell by treatment of metal oxide NPs (MO_x) with hexadecylphosphonic acid (PAC_{16}), the ligand shell was intercalated by the hydrophobic tail of a functional amphiphile, in this case SDBS (A^1) to yield the NP hybrid $[MO_x$-$(PAC_{16})]A^1$. Contrary to the hydrophobic

Chemistry–A European Journal

Review
doi.org/10.1002/chem.202000195

Chemistry Europe
European Chemical
Societies Publishing

first-shell NPs MO_x-(PAC$_{16}$), these NP hybrids display an orthogonally inverted polarity and thus dispersibility in aqueous media. Resulting from this architecture, a dynamic confined space between the two ligand shells can be utilized for the incorporation of hydrophobic guests (Figure 21), which was shown by a significantly increased hydrodynamic diameter of the particles upon treatment with nonpolar molecules. This concept was further extended by the implementation of ferromagnetic iron oxide (Fe_3O_4) as the core material. With Fe_3O_4 NPs, the intrinsic magnetic properties of the NP core were accessible after the *SbS*-functionalization of the material. Thus, the encapsulation of nonpolar molecules in the hydrophobic pocket of the NPs was combined with a magnetically driven separation of the loaded NPs from the water phase. The guest molecules could be released by treatment of the NPs with a nonpolar solvent through the absence of hydrophobic interactions. After further separation of the NPs, gas chromatography–mass spectrometry (GCMS) analysis provided insight into the extraction capacity of the SbS-coated NP hybrids. These measurements showed a varying affinity to different nonpolar molecules that ranged from 104 to 411% of the weight of the NPs. According to the findings of Halik,[14b] we attributed this to the different densities and stacking properties of the molecules. In comparison with other methods for the NP-based extraction of nonpolar molecules, this approach combines the outstanding aqueous dispersibility of the SbS-coated NPs and a high loading capacity through a micelle-like arrangement in between the two ligand shells with the intrinsic magnetic properties of Fe_3O_4 NPs.

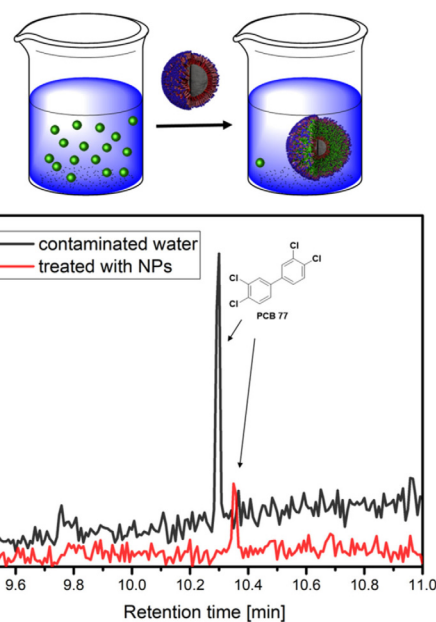The outstanding aqueous dispersibility of the [Fe_3O_4-(PAC$_{16}$)]A^1 enabled the extension of this concept towards the removal of PCBs from water sources. By treatment of a contaminated water source with [Fe_3O_4-(PAC$_{16}$)]A^1 a 75% reduction of the 3,3′,4,4′-tetrachlorbiphenyl (PCB 77) contamination was reached (Figure 22).

Figure 22. Extracted ion count GC/MS spectrum ($m/z = 292$) of a water sample contaminated with PCB 77 (black) and a PCB contaminated water sample treated with [TiO_2-(PAC$_{16}$)]A^1 (red). Reproduced from Ref. [1c]. Copyright 2019, Wiley-VCH.

applications. Therefore, Au-Fe_3O_4 nano-heterodimers (NHDs) were *SbS*-functionalized and were furthermore used for biological and medicinal applications, like radiation therapy against cancer.[1e] The Au-Fe_3O_4 nanocomposite is such an highly interesting material for radiation-based cancer therapies, because on the one hand side, Au NPs enhance X-radiation dosage at the tumor side and on the other side, the superparamagnetic iron oxide NPs (SPIONs) are known to generate highly reactive surfaces by irradiation with X-rays, composed of freed Fe^{3+} and Fe^{2+} ions, which facilitate the Haber-Weiss and Fenton process.[45] Hydrophobic Au-Fe_3O_4 NHDs were synthesized by thermal decomposition of iron oleate on pre-synthesized gold NPs and were further modified with the SbS-coating procedure using 1-octadecylpyridinium to provide a positive surface charge, or 4-dodecylbenzenezsulfonate to provide a negative surface charge.[1e] Through studies with human tumor (MCF-F7) and healthy epithelial (MCF-10A) cells, it was figured out that the surface charge and architecture of the NHDs influence the mechanism and efficiency of the cellular uptake pathway, cellular localization, and toxicity.[1e] SbS-structured NPs have the big advantage that initially hydrophobic coated NPs could be transferred to aqueous media by applying an amphiphile as a second shell building block and thus, also the surface charge of the NPs could be adjusted by choice of the amphiphile.

Figure 21. Schematic representation of the SbS-coated nanocarrier assemblies that reversibly bind guest molecules through hydrophobic interactions. Inorganic NP core: TiO_2 or Fe_3O_4. Reproduced from Ref. [1c]. Copyright 2019, Wiley-VCH.

Biomedicinal therapeutics

In general, SbS-functionalized NPs with amphiphiles containing a polar headgroup exhibit of excellent dispersibility and stability in water, which opens the door for biological and medicinal

Concluding Remarks

The chemistry of highly integrated nanomaterials consisting of a combination of organic and inorganic building blocks is currently an emerging field at the interface of synthetic chemistry, nanotechnology, and materials science. Both, covalent and noncovalent functionalization of metal oxide NPs with organic

phosphonic acids and amphiphiles, forming the basis for the hierarchical shell-by-shell functionalization, allows for systematic modification on the NP properties. This is directly reflected by the improvement and controlled modification of dispersibility and stability in various solvents giving rise to hydrophilicity, lipophilicity or fluorophilicity. This also prevents aggregation and Ostwald ripening. Also, optoelectronic properties of photoactive building blocks integrated within these hybrid architectures can be modulated. This can be achieved by adjustable nano-compartmentalization, an opportunity, which is an attractive consequence of the overall construction principle. Beyond the disclosure of these fundamental supramolecular properties also some first potential applications have been described. These include the development of water-cleaning materials. Another field of interest are magnetic SbS-functionalized Au/Fe_3O_4-nanoheterodimers as biomedicinal therapeutics for radiation therapy against cancer cells. With the SbS-functionalization concept, real tailor-made NPs can be produced, since a large variety of components (inorganic NPs, functional organic molecules forming the ligand shells) can be freely combined in a Lego-type manner. The NPs themselves bring along various properties, depending on the elemental composition, size, and shape. The organic ligands, such as phosphonic acids, can be fluorophilic, lipophilic, or hydrophilic and can further contain integrated functional units. Also, the selection of the amphiphile forming the second ligand shell brings along tunable properties. At this time first approaches have been introduced where SbS-architectures were transferred onto nanoporous flat surfaces, which opens additional doors for future applications.

Conflict of interest

The authors declare no conflict of interest.

[1] a) L. Zeininger, S. Petzi, J. Schönamsgruber, L. Portilla, M. Halik, A. Hirsch, *Chem. Eur. J.* **2015**, *21*, 14030–14035; b) L. Zeininger, L. M. S. Stiegler, L. Portilla, M. Halik, A. Hirsch, *ChemistryOpen* **2018**, *7*, 282–287; c) T. Luchs, M. Sarcletti, L. Zeininger, L. Portilla, C. Fischer, S. Harder, M. Halik, A. Hirsch, *Chem. Eur. J.* **2018**, *24*, 13589–13595; d) J. E. Wittmann, L. M. S. Stiegler, C. Henkel, J. Träg, K. Götz, T. Unruh, D. Zahn, A. Hirsch, D. Guldi, M. Halik, *Adv. Mater. Interfaces* **2019**, *6*, 1801930; e) S. Klein, L. M. S. Stiegler, C. Harreiss, L. V. R. Distel, W. Neuhuber, E. Spiecker, A. Hirsch, C. Kryschi, *ACS Appl. Bio Mater.* **2018**, *1*, 2002–2011.

[2] J. Shimoiizaka, K. Nakatsuka, T. Fujita, A. Kounosu, *IEEE Trans. Magn.* **1980**, *16*, 368–371.

[3] A. Wooding, M. Kilner, D. B. Lambrick, *J. Colloid Interface Sci.* **1991**, *144*, 236–242.

[4] L. Shen, P. E. Laibinis, T. A. Hatton, *Langmuir* **1999**, *15*, 447–453.

[5] a) N. Lala, S. P. Lalbegi, S. D. Adyanthaya, M. Sastry, *Langmuir* **2001**, *17*, 3766–3768; b) Y. Wang, J. F. Wong, X. Teng, X. Z. Lin, H. Yang, *Nano Lett.* **2003**, *3*, 1555–1559.

[6] a) E. Bilensoy, O. Gürkaynak, A. L. Doğan, A. A. Hıncal, *Int. J. Pham.* **2008**, *347*, 163–170; b) E. Bilensoy, A. A. Hincal, *Expert Opin. Drug Delivery* **2009**, *6*, 1161–1173; c) G. Varan, C. Varan, N. Erdoğan, A. Hıncal, E. Bilensoy, *Int. J. Pham.* **2017**, *531*, 457–469.

[7] a) A. Swami, A. Kumar, M. Sastry, *Langmuir* **2003**, *19*, 1168–1172; b) M. Hu, Y. Yamaguchi, T. Okubo, *J. Nanopart. Res.* **2005**, *7*, 187–193; c) Y. Lee, J. Jang, J. Yoon, J. W. Choi, I. Choi, T. Kang, *Chem. Commun.* **2019**, *55*, 3195–3198.

[8] a) M. Bruchez, Jr., M. Moronne, P. Gin, S. Weiss, A. P. Alivisatos, *Science* **1998**, *281*, 2013–2016; b) X. Wu, H. Liu, J. Liu, K. N. Haley, J. A. Treadway, J. P. Larson, N. Ge, F. Peale, M. P. Bruchez, *Nat. Biotechnol.* **2003**, *21*, 41–46; c) D. Deng, L. Qu, Y. Gu, *J. Mater. Chem. C* **2014**, *2*, 7077–7085; d) A. M. Smith, X. Gao, S. Nie, *Photochem. Photobiol.* **2004**, *80*, 377–385; e) W. W. Yua, E. Chang, R. Drezek, V. L. Colvin, *Biochem. Biophys. Res. Commun.* **2006**, *348*, 781–786; f) J. M. Klostranec, W. C. W. Chan, *Adv. Mater.* **2006**, *18*, 1953–1964; g) C. A. Lin, R. A. Sperling, J. K. Li, T. Y. Yang, P. Y. Li, M. Zanella, W. H. Chang, W. J. Parak, *Small* **2008**, *4*, 334–341.

[9] T. Pellegrino, L. Manna, S. Kudera, T. Liedl, D. Koktysh, A. L. Rogach, S. Keller, J. Raedler, G. Natile, W. J. Parak, *Nano Lett.* **2004**, *4*, 703–707.

[10] R. A. Sperling, W. J. Parak, *Phil. Trans. R. Soc. A* **2010**, *368*, 1333–1383.

[11] L. M. S. Stiegler, A. Hirsch, *Chem. Eur. J.* **2019**, *25*, 11864–11875.

[12] a) J. Bai, B. Zhou, *Chem. Rev.* **2014**, *114*, 10131–10176; b) Y. Bai, I. Mora-Sero, F. De Angelis, J. Bisquert, P. Wang, *Chem. Rev.* **2014**, *114*, 10095–10130.

[13] a) K. D. Bakoglidis, K. Simeonidis, D. Sakellari, G. Stefanou, M. Angelakeris, *IEEE T. Magn.* **2012**, *48*, 1320–1323; b) A. Akbarzadeh, M. Samiei, S. Davaran, *Nanoscale Res. Lett.* **2012**, *7*, 144; c) K. Woo, J. Hong, S. Choi, H.-W. Lee, J.-P. Ahn, C. S. Kim, S. W. Lee, *Chem. Mater.* **2004**, *16*, 2814–2818.

[14] a) T. Luchs, P. Lorenz, A. Hirsch, *ChemPhotoChem* **2020**, *4*, 52–58; b) M. Sarcletti, D. Vivod, T. Luchs, T. Rejek, L. Portilla, L. Müller, H. Dietrich, A. Hirsch, D. Zahn, M. Halik, *Adv. Funct. Mater.* **2019**, *29*, 1805742.

[15] a) L. Portilla, M. Halik, *ACS Appl. Mater. Interfaces* **2014**, *6*, 5977–5982; b) P. J. Hotchkiss, S. C. Jones, S. A. Paniagua, A. Sharma, B. Kippelen, N. R. Armstrong, S. R. Marder, *Acc. Chem. Res.* **2012**, *45*, 337–346.

[16] S. P. Pujari, L. Scheres, A. T. Marcelis, H. Zuilhof, *Angew. Chem. Int. Ed.* **2014**, *53*, 6322–6356; *Angew. Chem.* **2014**, *126*, 6438–6474.

[17] L. Zeininger, L. Portilla, M. Halik, A. Hirsch, *Chem. Eur. J.* **2016**, *22*, 13506–13512.

[18] a) R. Hofer, M. Textor, N. D. Spencer, *Langmuir* **2001**, *17*, 4014–4020; b) T. J. Daou, S. Begin-Colin, J. M. Grenèche, F. Thomas, A. Derory, P. Bernhardt, P. Legaré, G. Pourroy, *Chem. Mater.* **2007**, *19*, 4494–4505; c) P. H. Mutin, G. Guerrero, A. Vioux, *J. Mater. Chem.* **2005**, *15*, 3761–3768; d) G. Guerrero, P. H. Mutin, A. Vioux, *Chem. Mater.* **2001**, *13*, 4367–4373; e) P. H. Mutin, G. Guerrero, A. Vioux, *C. R. Chim.* **2003**, *6*, 1153–1164; f) G. Guerrero, J. G. Alauzun, M. Granier, D. Laurencin, P. H. Mutin, *Dalton Trans.* **2013**, *42*, 12569–12585; g) Y. Sahoo, H. Pizem, T. Fried, D. Golodnitsky, L. Burstein, C. N. Sukenik, G. Markovich, *Langmuir* **2001**, *17*, 7907–7911; h) M. Higo, S. Kamata, *J. Phys. Chem.* **1990**, *94*, 8709–8714; i) A. Garofalo, A. Parat, C. Bordeianu, C. Ghobril, M. Kueny-Stotz, A. Walter, J. Jouhannaud, S. Begin-Colin, D. Felder-Flesch, *New J. Chem.* **2014**, *38*, 5226–5239; j) V. Zoulalian, S. Zürcher, S. Tosatti, M. Textor, S. Monge, J.-J. Robin, *Langmuir* **2010**, *26*, 74–82; k) V. Zoulalian, S. Monge, S. Zürcher, M. Textor, J. J. Robin, S. Tosatti, *J. Phys. Chem. B* **2006**, *110*, 25603–25605; l) D. Brovelli, G. Hähner, L. Ruiz, R. Hofer, G. Kraus, A. Waldner, J. Schlösser, P. Oroszlan, M. Ehrat, N. D. Spencer, *Langmuir* **1999**, *15*, 4324–4327; m) H. B. Liu, N. V. Venkataraman, N. D. Spencer, M. Textor, S. J. Xiao, *ChemPhysChem* **2008**, *9*, 1979–1981; n) D. M. Spori, N. V. Venkataraman, S. G. P. Tosatti, F. Durmaz, N. D. Spencer, S. Zürcher, *Langmuir* **2007**, *23*, 8053–8060; o) Y. Lalatonne, M. Monteil, H. Jouni, J. M. Serfaty, O. Sainte-Catherine, N. Lievre, S. Kusmia, P. Weinmann, M. Lecouvey, L. Motte, *J. Osteoporos.* **2010**, *2010*, 1; p) E.

Guénin, Y. Lalatonne, J. Bolley, I. Milosevic, C. Platas-Iglesias, L. Motte, *J. Nanopart. Res.* **2014**, *16*, 2596.

[19] a) C. Queffélec, M. Petit, P. Janvier, D. A. Knight, B. Bujoli, *Chem. Rev.* **2012**, *112*, 3777–3807; b) K. J. Gagnon, H. P. Perry, A. Clearfield, *Chem. Rev.* **2012**, *112*, 1034–1054.

[20] a) T. Hauffman, O. Blajiev, J. Snauwaert, C. v. Haesendonck, A. Hubin, H. Terryn, *Langmuir* **2008**, *24*, 13450–13456; b) X. Chen, E. Luais, N. Darwish, S. Ciampi, P. Thordarson, J. J. Gooding, *Langmuir* **2012**, *28*, 9487–9495.

[21] H.-Y. Nie, M. J. Walzak, N. S. McIntyre, *J. Phys. Chem. B* **2006**, *110*, 21101–21108.

[22] G. Guerrero, P. H. Mutin, A. Vioux, *J. Mater. Chem.* **2001**, *11*, 3161–3165.

[23] N. Griep-Raming, M. Karger, H. Menzel, *Langmuir* **2004**, *20*, 11811–11814.

[24] a) S. Marcinko, A. Y. Fadeev, *Langmuir* **2004**, *20*, 2270–2273; b) T. Lenz, T. Schmaltz, M. Novak, M. Halik, *Langmuir* **2012**, *28*, 13900–13904; c) K. Y. Foo, B. H. Hameed, *Chem. Eng. J.* **2010**, *156*, 2–10; d) J. De Roo, Y. Justo, K. De Keukeleere, F. Van den Broeck, J. C. Martins, I. Van Driessche, Z. Hens, *Angew. Chem. Int. Ed.* **2015**, *54*, 6488–6491; *Angew. Chem.* **2015**, *127*, 6588–6591.

[25] a) H. Klauk, U. Zschieschang, J. Pflaum, M. Halik, *Nature* **2007**, *445*, 745–748; b) S. Tosatti, R. Michel, M. Textor, N. D. Spencer, *Langmuir* **2002**, *18*, 3537–3548; c) S. A. Paniagua, P. J. Hotchkiss, S. C. Jones, S. R. Marder, A. Mudalige, F. S. Marrikar, J. E. Pemberton, N. R. Armstrong, *J. Phys. Chem. C* **2008**, *112*, 7809–7817.

[26] R. Campos, A. J. Guenthner, T. S. Haddad, J. M. Mabry, *Langmuir* **2011**, *27*, 10206–10215.

[27] L. Nebhani, D. Schmiedl, L. Barner, C. Barner-Kowollik, *Adv. Funct. Mater.* **2010**, *20*, 2010–2020.

[28] L. Zeininger, M. Klaumuenzer, W. Peukert, A. Hirsch, *Int. J. Mol. Sci.* **2015**, *16*, 8186–8200.

[29] W. Lin, J. Walter, A. Burger, H. Maid, A. Hirsch, W. Peukert, D. Segets, *Chem. Mater.* **2014**, *26*, 358–369.

[30] a) G. Garnweitner, H. O. Ghareeb, C. Grote, *Colloids Surf. A Physicochem. Eng. Asp.* **2010**, *372*, 41–47; b) D. Sun, J. Wong, L. Sun, Y. Li, N. Miyatake, H.-J. Sue, *J. Sol-Gel Sci.Technol.* **2007**, *43*, 237–243; c) Y. A. Wang, J. J. Li, H. Chen, X. Peng, *J. Am. Chem. Soc.* **2002**, *124*, 24.

[31] D. Traini, P. Rogueda, P. Young, R. Price, *Pharm. Res.* **2005**, *22*, 816–825.

[32] a) C. J. Van Oss, R. J. Good, K. Chaudhury, *Langmuir* **1988**, *4*, 884–891; b) C. J. Van Oss, R. J. Good, R. J. Busscher, *J. Disper. Sci. Technol.* **1990**, *11*, 75–81.

[33] J. J. Jasper, E. V. Kring, *J. Phys. Chem.* **1955**, *59*, 1019–1021.

[34] a) R. Förch, H. Schönherr, A. T. A. Jenkins, *Surface Design: Applications in Bioscience and Nanotechnology*, Wiley-VCH, Weinheim, **2009**, p.444; b) F. M. Fowkes, *Contact Angle, Wettability, and Adhesion, J. Am. Chem. Soc., Adv. Chem. Ser. 43*, Washington, DC, **1964**; c) L. Feng, S. Li, Y. Li, H. Li, L. Zhang, J. Zhai, Y. Song, B. Liu, L. Jiang, D. Zhu, *Adv. Mater.* **2002**, *14*, 1857–1860.

[35] M. Gliboff, H. Li, K. M. Knesting, A. J. Giordano, D. Nordlund, G. T. Seidler, J.-L. Brédas, S. R. Marder, D. S. Ginger, *J. Phys. Chem. C* **2013**, *117*, 15139–15147.

[36] W. Al-Shatty, A. M. Lord, S. Alexander, A. R. Barron, *ACS Omega* **2017**, *2*, 2507–2514.

[37] a) J. B. Birks, L. G. Christophorou, *Nature* **1963**, *197*, 1064–1065; b) J. B. Birks, *J. Phys. Chem.* **1963**, *67*, 2199–2200; c) J. B. Birks, L. G. Christophorou, *Spectrochim. Acta* **1962**, *18*, 363; d) J. B. Birks, L. G. Christophor-

ou, *Spectrochim. Acta* **1963**, *19*, 401–410; e) B. Stevens, E. Hutton, *Nature* **1960**, *186*, 1045–1046.

[38] a) J. Träg, D. Zahn, *J. Mol. Model.* **2019**, *25*, 39; b) L. M. Wilson, A. C. Griffin, *Macromolecules* **1993**, *26*, 6312–6314; c) L. M. Wilson, A. C. Griffin, *Macromolecules* **1994**, *27*, 1928–1931.

[39] a) D. A. Wade, C. Mao, A. C. Hollenbeck, S. A. Tucker, *Frenzius J. Anal. Chem.* **2001**, *369*, 378–384; b) D. A. Wade, S. A. Tucker, *Talanta* **2000**, *53*, 571–578; c) S. Pandey, W. E. Acree, Jr., J. C. Fetzer, *Mikrochim. Acta* **1998**, *129*, 41–45; d) S. Pandey, W. E. Acree, Jr., C. Fetzer, *Talanta* **1998**, *47*, 769–778; e) S. Pandey, W. E. Acree, Jr., C. Fetzer, *Talanta* **1997**, *45*, 39–45.

[40] L. Zhong, F. Xing, W. Shi, L. Yan, S. Xie, S. Zhu, *ACS Appl. Mater. Interfaces* **2013**, *5*, 3401–3407.

[41] a) B. J. Coe, *Acc. Chem. Res.* **2006**, *39*, 383–393; b) R. C. Vieira, D. E. Falvey, *J. Am. Chem. Soc.* **2008**, *130*, 1552–1553; c) D. Behar, P. Neta, C. Schultheisz, *J. Phys. Chem. A* **2002**, *106*, 3139–3147; d) A. Skrzypczak, P. Neta, *J. Phys. Chem. A* **2003**, *107*, 7800–7803; e) A. G. Peroff, E. Weitz, R. P. Van Duyne, *Phys. Chem. Chem. Phys.* **2016**, *18*, 1578–1586; f) M. Z. Ertem, S. J. Konezny, C. M. Araujo, V. S. Batista, *J. Phys. Chem. Lett.* **2013**, *4*, 745–748; g) Y. Yan, E. L. Zeitler, J. Gu, Y. Hu, A. B. Bocarsly, *J. Am. Chem. Soc.* **2013**, *135*, 14020–14023.

[42] a) M. Gias Uddin, A. T. M. Z. Azam, *Am. J. Biochem. Mol. Biol.* **2013**, *3*, 175–181; b) C. E. Agudelo-Morales, R. E. Galian, J. Pérez-Prieto, *Anal. Chem.* **2012**, *84*, 8083–8087.

[43] a) S. C. Bagby, C. M. Reddy, C. Aeppli, G. B. Fisher, D. L. Valentine, *Proc. Natl. Acad. Sci. USA* **2017**, *114*, E9–E18; b) M. K. McNutt, R. Camilli, T. J. Crone, G. D. Guthrie, P. A. Hsieh, T. B. Ryerson, O. Savas, F. Shaffer, *Proc. Natl. Acad. Sci. USA* **2012**, *109*, 20260–20267; c) E. Malaj, P. C. von der Ohe, M. Grote, R. Kuhne, C. P. Mondy, P. Usseglio-Polatera, W. Brack, R. B. Schafer, *Proc. Natl. Acad. Sci. USA* **2014**, *111*, 9549–9554; d) B. McHugh, R. Poole, J. Corcoran, P. Anninou, B. Boyle, E. Joyce, M. Barry Foley, E. McGovern, *Chemosphere* **2010**, *79*, 305–313.

[44] a) Q. Zhu, F. Tao, Q. Pan, *ACS Appl. Mater. Interfaces* **2010**, *2*, 3141–3146; b) Y. Chu, Q. Pan, *ACS Appl. Mater. Interfaces* **2012**, *4*, 2420–2425; c) P. Calcagnile, D. Fragouli, I. S. Bayer, G. C. Anyfantis, L. Martiradonna, P. D. Cozzoli, R. Cingolani, A. Athanassiou, *ACS Nano* **2012**, *6*, 5413–5419; d) S. Yang, L. Chen, L. Mu, P.-C. Ma, *J. Colloid Interf. Sci.* **2014**, *430*, 337–344; e) L. Yu, G. Hao, J. Gu, S. Zhou, N. Zhang, W. Jiang, *J. Magn. Magn. Mater.* **2015**, *394*, 14–21; f) O. Saber, N. H. Mohamed, S. A. Arafat, *RSC Adv.* **2015**, *5*, 72863–72871; g) M. Patowary, R. Ananthakrishnan, K. Pathak, *Environ. Sci. Pollut. Res. Int.* **2017**, *24*, 18063–18072; h) H.-Y. Mi, X. Jing, H. Xie, H.-X. Huang, L.-S. Turng, *Chem. Eng. J.* **2018**, *337*, 541–551.

[45] a) S. Klein, J. Hübner, C. Menter, L. Distel, W. Neuhuber, C. Kryschi, *Appl. Sci.* **2018**, *9*, 15; b) S. Klein, C. Harreiss, C. Menter, J. Hummer, L. V. R. Distel, K. Meyer, R. Hock, C. Kryschi, *ACS Appl. Mater. Interfaces* **2018**, *10*, 17071–17080; c) S. Klein, A. Sommer, L. V. Distel, W. Neuhuber, C. Kryschi, *Biochem. Biophys. Res. Commun.* **2012**, *425*, 393–397; d) S. Klein, A. Sommer, L. V. Distel, J. L. Hazemann, W. Kroner, W. Neuhuber, P. Müller, O. Proux, C. Kryschi, *J. Phys. Chem. B* **2014**, *118*, 6159–6166.